Power law behavior of the isotope yield distributions in the multifragmentation regime of heavy ion reactions

M. Huang,[1,2,3] R. Wada,[3,*] Z. Chen,[1,3] T. Keutgen,[4] S. Kowalski,[5] K. Hagel,[3] M. Barbui,[3] A. Bonasera,[3,6] C. Bottosso,[3] T. Materna,[3] J. B. Natowitz,[3] L. Qin,[3] M. R. D. Rodrigues,[3] P. K. Sahu,[3] K. J. Schmidt,[3] and J. Wang[1]

[1]*Institute of Modern Physics, Chinese Academy of Sciences, Lanzhou 730000, China*
[2]*Graduate University of Chinese Academy of Sciences, Beijing 100049, China*
[3]*Cyclotron Institute, Texas A&M University, College Station, Texas 77843, USA*
[4]*FNRS and IPN, Université Catholique de Louvain, B-1348 Louvain-Neuve, Belgium*
[5]*Institute of Physics, Silesia University, Katowice, Poland*
[6]*Laboratori Nazionali del Sud, INFN, via Santa Sofia, 62, I-95123 Catania, Italy*

(Received 27 July 2010; published 4 November 2010)

Isotope yield distributions in the multifragmentation regime were studied with high-quality isotope identification, focusing on the intermediate mass fragments (IMFs) produced in semiviolent collisions. The yields were analyzed within the framework of a modified Fisher model. Using the ratio of the mass-dependent symmetry energy coefficient relative to the temperature, $a_{\rm sym}/T$, extracted in previous work and that of the pairing term, $a_{\rm p}/T$, extracted from this work, and assuming that both reflect secondary decay processes, the experimentally observed isotope yields were corrected for these effects. For a given $I = N - Z$ value, the corrected yields of isotopes relative to the yield of ^{12}C show a power law distribution $Y(N, Z)/Y(^{12}\mathrm{C}) \sim A^{-\tau}$ in the mass range $1 \leqslant A \leqslant 30$, and the distributions are almost identical for the different reactions studied. The observed power law distributions change systematically when I of the isotopes changes and the extracted τ value decreases from 3.9 to 1.0 as I increases from -1 to 3. These observations are well reproduced by a simple deexcitation model, with which the power law distribution of the primary isotopes is determined to be $\tau^{\rm prim} = 2.4 \pm 0.2$, suggesting that the disassembling system at the time of the fragment formation is indeed at, or very near, the critical point.

DOI: 10.1103/PhysRevC.82.054602 PACS number(s): 25.70.Pq, 21.10.Dr, 21.65.Ef, 24.10.−i

I. INTRODUCTION

Since the late 70s, many charge or mass distributions observed in energetic collisions with a variety of projectiles from protons to heavy ions and in a wide range of incident energies from 15 A MeV to several A GeV have been fit using a power law ansatz. The Purdue Group demonstrated that the isotope yields of intermediate mass fragments (IMFs) produced in high-energy proton-nucleus collisions at Fermi Lab exhibited a power law distribution with a τ value of 2.64–2.65 [1–3]. This observation stimulated the studies of critical phenomena and phase transitions in nuclear matter. Trautmann *et al.* reported that the charge distributions from many published data fit with a power law show a systematic trend in the power law exponent as a function of the incident energy [4]. The exponent changes from $\tau \sim 7$ to 2 as the incident energy increases from 50 MeV to 1 GeV and more or less saturates at $\tau \sim 2$ above 1 GeV. They attributed the significant change in the value of τ at lower energy to the angular momentum effect on IMF emission. Work through the 90s to early 2000s is well summarized both from the experimental and theoretical point of views in Refs. [5,6]. In the mid 90s to 2000s, the Berkeley Group, applying Fisher's droplet-model concepts to the experiments performed by the EOS and ISIS Collaborations, argued that the disassembling system does indeed show a critical behavior [7–10]. They extracted a τ value of 2.2 ± 0.1 from both experiments.

One of the complications in multifragmentation originates from secondary statistical decay processes. When fragments are formed in a disassembling system, they are generally excited and most deexcite to the ground state by the time of detection [11–13]. According to Ref. [13], the average parent of $Z = 10$ fragments produced in the Xe + Sn reaction at 39 A MeV emits ∼5.5 mass units as ∼1.75 charged particles and an additional ∼4 mass units as neutrons. This secondary decay process significantly alters the fragment isotopic distribution. Studies using statistical decay codes also indicate that the primary fragment distributions are significantly modified during the secondary decay process [14,15]. Most multifragmentation models, statistical or dynamical, take this process into account, but the magnitude of the change depends on the codes and results can vary significantly [16]. In the analysis of the Purdue Group, the secondary decay process was not taken into account and data for $4 \leqslant A \leqslant 12$ were excluded from the fit in determining the τ values. This is true for most of the work published in the 80s and 90s. In addition, the data have rather large errors [4]. In the analysis of the Berkeley group, since no mass was identified in either of the experiments, the secondary effects were treated empirically. In their analysis, the mass of each isotope was calculated as $2Z[1 + y(E^*/B_f)]$, where E^* and B_f are the fragment excitation energy and ground-state binding energy, respectively, and y is a free parameter. The parameters were determined to establish the power law between the scaled cluster yield and the scaled temperature [9].

*wada@comp.tamu.edu

In order to get direct insight into the nature of the disassembling system at the time of fragment formation, it is preferable to determine the secondary effects experimentally in particle-fragment correlations and use that information to reconstruct the yields of primary isotopes. However, this is not straight forward since multiple fragments are generally produced in a reaction and light particles can be produced even before the formation of the fragments. Therefore, identification of the parent of detected light particles observed in coincidence with a fragment is not trivial [11–13]. Furthermore, neutrons are particularly difficult as the multiplicity of neutrons from the secondary decay of a particular IMF accounts for only a small fraction of the total neutron multiplicity.

In this work, we focus on an alternative method in which the observed isotope distributions are corrected for known secondary decay effects to extract information on the properties of the disassembling system at the time of fragment formation. In the following sections, isotopic yield distributions are studied for different values of $I = N - Z$ separately, elucidating the role of the secondary decay process in modifying the original fragment distribution and, in particular, its effect on determining the power law exponent τ of the emitting source. This article is organized as follows: In Sec. II, the experiment and analysis procedures are briefly described. In Sec. III, a modified Fisher model is described. In Sec IV, the corrected isotope yield distributions are presented for $I = 0$ and $I \neq 0$ separately. In Sec. V, a possible explanation is presented for the observed systematic trend of the τ values, using a simple cascade model. A brief summary is given in Sec. VI.

II. EXPERIMENT AND DATA ANALYSIS

The experiment was performed at the K-500 superconducting cyclotron facility at Texas A&M University. Beams of 40-A-MeV ^{64,70}Zn and ^{64}Ni were used to irradiate ^{58,64}Ni, ^{112,124}Sn, ^{197}Au, and ^{232}Th targets. IMFs were measured at 20° and typically 6–8 isotopes for atomic numbers Z up to $Z = 18$ were clearly identified. The yields of light charged particles (LCPs) in coincidence with IMFs were also measured using 16 single-crystal CsI(Tl) detectors. The details of the experiments and the data analysis can be found in Refs. [17,18].

In the experiment, IMFs were measured using a 5 × 5-cm^2 quadrant Si telescope and the detection angle was carefully chosen. The angle should be small enough so that sufficient IMF yields are obtained above the detector energy threshold, but large enough so that the contribution from peripheral collisions is negligible. For this purpose, simulations of the antisymmetrized molecular dynamics model (AMD) [19,20] incorporating a statistical decay code GEMINI [21] as an afterburner (used in the previous work [22]) were employed. The simulations are also used to elucidate the impact-parameter range sampled and the IMF production mechanism involved in the present data set. In Fig. 1, calculated impact-parameter distributions are presented for the ^{64}Zn + ^{112}Sn system. The violence of the reaction for each event is determined in the same way as in the previous work [22], in which the multiplicity of light particles, including neutrons, and the transverse energy of light charged particles were used. The resultant impact-parameter distributions are shown for each class of

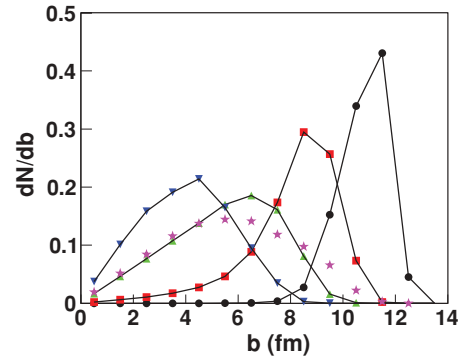

FIG. 1. (Color online) Simulated impact parameter distributions for violent (downward triangles), semiviolent (upward triangles), semiperipheral (squares), and peripheral (dots) collisions. Stars indicate the events in which at least one IMF ($Z \geqslant 3$) is emitted at 20° ± 5°. The summed distribution for a given class is normalized to 1.

events together with that of the events in which at least one IMF is emitted at an angle of 20° ± 5°. As seen in the figure, the distribution of the events selected by the IMF detection is very similar to that of semiviolent collisions which have a broad impact-parameter distribution overlapping significantly with that of the violent collisions. In these events, the semiperipheral and peripheral collisions are significantly suppressed.

In order to further isolate the reaction mechanisms involved in the reaction products, a moving-source fit was employed. For light particles, three sources were used: the projectile-like (PLF), the intermediate-velocity (IV), and the target-like (TLF) sources. For IMFs, a single IV source was used to extract the multiplicity. In Fig. 2, the experimental energy spectra of ^{16}O are compared with the result of those from the AMD + GEMINI calculation on an absolute scale, together

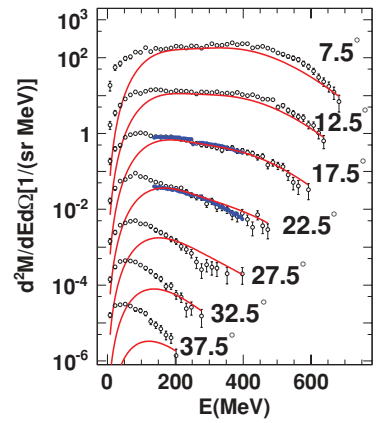

FIG. 2. (Color online) Experimental ^{16}O energy spectra (closed circles) are compared with the AMD + GEMINI result (open circles) for ^{64}Zn + ^{112}Sn at 40 A MeV. The spectra for the AMD + GEMINI result is obtained for the semiviolent collisions. Detection angles are given in the figure and the absolute Y scale corresponds to the bottom spectra and the spectra are multiplied by a factor of 10 from the bottom to the top. The curves are the result of the moving-source fit, in which the parameters are determined from the experimental spectra at 17.5° and 22.5°. The source velocity of $V_s = 0.62V_p$ and $\Delta V_s = 0.11V_p$ are used.

with the moving-source fit result. The spectra for the AMD + GEMINI result are those corresponding to the semiviolent collisions. The experimental spectra at 17.5° and 22.5° are well reproduced by the AMD + GEMINI simulation. The moving-source parameters were determined from the experimental spectra. For IMFs, a fixed apparent temperature of 17 MeV was used. The IV source velocity was smeared between $V_s \pm \Delta V_s$. Typically, $V_s = 0.6V_p$ and $\Delta V_s = 0.1V_p$ were used, where V_p is the projectile velocity, but for each case these values were optimized. The majority of the spectra at angles $\theta \leqslant 20^\circ$ are well reproduced by the IV source component, except for the lower energy side of these spectra and those at $\theta \geqslant 25^\circ$. These are attributed to the TLF component. One can also see a small enhancement in the AMD + GEMINI result above the moving-source fit at forward angles, which is attributed to the PLF source component. For the semiperipheral or peripheral collisions, a prominent PLF component with the source velocity, $V_s \sim 0.9V_p$ appears at forward angles. These are generally observed for all isotopes measured in all reactions presented here. The PLF and TLF source components are not taken into account in the present analysis. Therefore the IMF multiplicities presented in this work are those of the IV source component. As seen below, the isotope distribution for different reaction systems show almost identical features, after certain corrections are made, even though the reactions studied are quite different. This indicates that the production mechanism for the IMFs, selected by the setup of the detector angle and the selection of the IV source component, are indeed very similar for systems studied. This will be further discussed in Sec. V.

In Fig. 3, the multiplicity distributions of the observed isotopes are plotted as a function of A for the case of the ^{64}Ni projectile on different targets. The data are plotted from top to bottom as N/Z of the target increases. The distributions roughly show a power law distribution up to $A = 30$. Above $A = 30$, the multiplicity decreases sharply for all cases. In the figure, the distributions are fit by a power law distribution

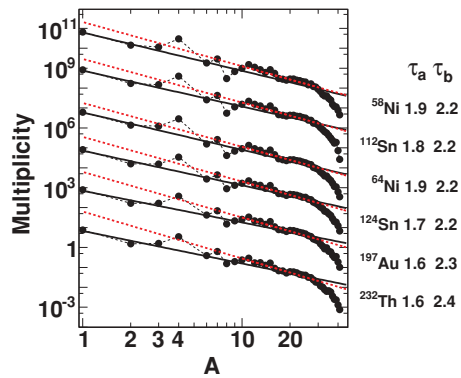

FIG. 3. (Color online) Experimental multiplicity distributions vs. isotope mass A for the ^{64}Ni projectiles with different targets. Targets are indicated on the right for each distribution. Each datum represents a summed multiplicity over Z for a given A. Solid lines are the resits of power law fits for $1 \leqslant A \leqslant 30$ and dotted lines are for $10 < A \leqslant 30$. The extracted τ values are also given as τ_a and τ_b, respectively. The absolute multiplicity value is given for the distribution at the bottom reaction and the multiplicity is multiplied by a factor of 100 from the bottom to the top.

$A^{-\tau}$ in two different ranges of A, one (solid lines, τ_a) is obtained with $1 \leqslant A \leqslant 30$ and the other (dotted lines, τ_b) with $10 \leqslant A \leqslant 30$. In the latter cases, the extracted values are in the range of 2.2 to 2.4, and slowly increase as N/Z of the target increases. The values are slightly smaller than those extracted by the Purdue group [1–3], which were extracted from a similar range of A. On the other hand, when the distributions are fit over a wider range extended to $A = 1$, the extracted τ values becomes smaller ($1.6 \leqslant \tau \leqslant 1.9$) and decrease when the target N/Z increases. In both cases, the data fluctuate along the fitted lines for smaller IMFs. The yields for $A = 4$ are always higher than the fit lines, and $A = 8$ yields are significantly lower. For other reaction systems, similar results are observed. These observations suggest that the secondary decay process plays a significant role in these distributions. To elucidate the role of the secondary decay process, the multiplicity distributions are examined in detail, using information from the wide variety of isotopes identified in this experiment.

In the previous work of Ref. [17], we extracted the ratio between the symmetry energy coefficient and the temperature, a_{sym}/T, from the isobaric yield ratios of IMFs in a given reaction, based on the modified Fisher model [2,3]. In another work (Ref. [18]), the a_{sym}/T values are evaluated by two other independent methods. One uses isoscaling parameters determined from the ratio of the isotope yields between two different reactions. The other employs the variance of the isotope-yield distribution in a single reaction. All results from the three different methods are in reasonable agreement and indicate that the extracted values of a_{sym}/T depend significantly on the mass number A of the fragment (i.e., a_{sym}/T gradually increases from $4 \sim 6$ to $12 \sim 16$ as A increases from 9 to 37). These values depend slightly on the different methods, but the essential trends are quite similar. The extracted values can be empirically fit by

$$\begin{aligned} a_{sym}^{emp}/T &= 5 + 1.4(A-9)^{\frac{2}{3}} \quad \text{for } A \geqslant 9 \\ &= 5 \quad \text{for } A < 9. \end{aligned} \tag{1}$$

In those articles, detailed comparisons to AMD-model simulations [19,20] incorporating a statistical decay code GEMINI [21] as an afterburner show that the experimentally observed A dependence is very well reproduced. In contrast, the a_{sym}/T values extracted from the primary isotope yield distributions of the AMD calculations, before cooling with the afterburner, are nearly constant with $a_{sym}/T \sim 4$ to 6 (depending on the extraction method) over the mass range of the observed isotopes, indicating that the experimentally observed A dependence of the symmetry-energy term originates from the secondary statistical decay of the excited primary fragments.

III. MODIFIED FISHER MODEL

The modified Fisher model of Refs. [2,3] has been used to study the isotopic distributions of the fragments. In this model, the yield $Y(A, I)$ of A nucleons with $I = N - Z$ is given by

$$Y(A, I) = CA^{-\tau} \exp\left\{\frac{F(A, I, T, \rho) + \mu_n N + \mu_p Z}{T} + N\ln(N/A) + Z\ln(Z/A)\right\}, \tag{2}$$

where C is a constant. The $A^{-\tau}$ factor originates from the entropy of the fragment. The quantities μ_n and μ_p are the neutron and proton chemical potentials, respectively. The last two terms are from the entropy of mixing of neutrons and protons [23]. The function $F(A, I, T, \rho)$ is the free energy of the cluster at temperature T and density ρ.

Since the isotope yields of IMFs have been evaluated for the nucleon-nucleon (IV) source component, the same component in the light-charged-particle emission is also used. This is evaluated in Ref. [17,18]. In order to compare the yields for different reaction systems, all yields are normalized to that of ^{12}C in a given system.

IV. RESULTS

A. Isotopes with $I = 0$

We study separately the isotope yields for $I = 0$ and $I \neq 0$. For the isotopes with $I = 0$, the symmetry energy contribution in Eq. (2) becomes zero. Since these isotopes can be even-even or odd-odd nuclei, the yields of odd-odd and even-even $I = 0$ isotopes are plotted separately as a function of A in the top and middle of Fig. 4 for the 13 different reactions studied. In each case, the distributions from the different reactions are almost identical. They show a power law behavior up to $A \sim 30$. The extracted values of τ are $\tau = 3.3$ for even-even and $\tau = 2.2$ for odd-odd. The difference in slopes might naturally be attributed to pairing effects. While large pairing effects are expected at low temperatures because they are related to shell effects [24], the disassembling system is initially at a high temperature. Ricciardi *et al.* have suggested an explanation for the apparent strong effect of pairing in such systems [25,26]. According to their model simulations, experimentally observed pairing effects may be attributed to the last-chance particle decay of the excited fragments during cooling. This hypothesis is also supported by our model simulations presented in Ref. [17]. We therefore treat the observed pairing effect as one of the secondary decay effects.

By fitting the yields of even-even and odd-odd isotopes simultaneously and including the pairing coefficient a_p in the fitting process, we obtain $\tau = 2.9$ (bottom panel of Fig. 4) and $a_p/T = 2.2$. Using these parameters, we have divided the normalized yields by the pairing energy contribution, $\exp(\delta/T)$, in which $\delta = a_p/A^{\frac{1}{2}}$ for even-even, $\delta = 0$ for even-odd, and $\delta = -a_p/A^{\frac{1}{2}}$ for odd-odd isotopes. The resultant corrected isotope distribution is shown with a fitted line in the bottom figure for all isotopes with $I = 0$.

B. Isotopes with $I \neq 0$

For the isotopes with $I \neq 0$, one can write the free energy as

$$F(A, I, T, \rho) = F'(A, I = 0, T, \rho) - a_{\rm sym} I^2/A + \delta(N, Z). \quad (3)$$

This formulation indicates that the pairing term for $I = 0$ is excluded and added explicitly into Eq. (3). Since the symmetry contribution is larger for larger I values, we first examine the isotopes with $I = 3$, which is the largest I value for which

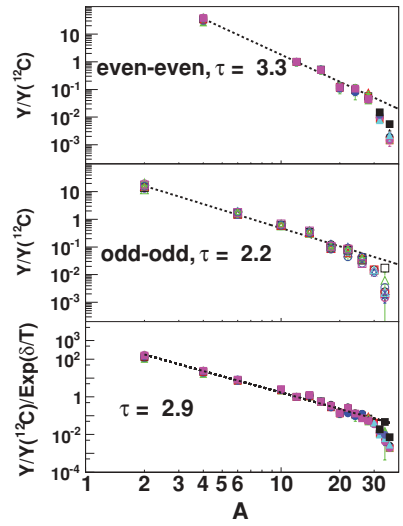

FIG. 4. (Color online) (Upper) $Y/Y(^{12}C)$ as a function of A for even-even isotopes with $I = 0$. (Middle) Same as the upper, but for odd-odd isotopes with $I = 0$. (Bottom) The pairing energy term corrected yields for isotopes with $I = 0$. The lines are the results fit by $A^{-\tau}$. The extracted τ values are shown in each figure.

the yields of a reasonable number of isotope species have been determined. In this case, all isotopes are even-odd and therefore the pairing term drops out of Eq. (3). The corrected isotope distributions obtained from the normalized yields divided by $\exp(-E^{\rm emp}_{\rm sym}/T)$ are plotted as a function of A in Fig. 5 for all reactions. Here $E^{\rm emp}_{\rm sym} = a^{\rm emp}_{\rm sym} I^2/A$ and $a^{\rm emp}_{\rm sym}$ is given by Eq. (1). One can make a few distinct observations. First, there is a clear even-odd effect. This indicates that the pairing effects can originate not only from the last-chance particle decay, but also from the second-to-last particle decay; the latter in lesser magnitude, as discussed in Ref. [17]. In other words, the parents of $I = 3$ isotopes can be $I = 2$ isotopes in the cooling path and the pairing effects are carried on to the $I = 3$ isotopes.

Another observation is a poor scaling between different reactions. Although the distribution does not scale well in magnitude, it is noted that the shapes of the distributions are

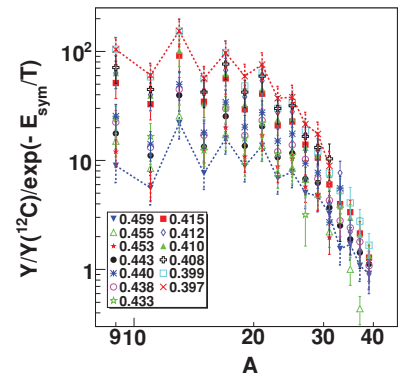

FIG. 5. (Color online) Symmetry-term-corrected yields of $I = 3$ for different reaction systems. Different symbols present different reactions. Dotted lines are connected between data points for the smallest and largest Z/A values, respectively.

very similar to each other, especially in the mass range up to $A = 25$. This suggests slight differences between the emitting sources in the different reaction systems. In Eq. (2), for a given isotope, the difference between different reactions comes through the chemical potential terms $(\mu_n N + \mu_p Z)/T$. As pointed out in Ref. [27], the experimental results indicate a relation between isotopic scaling parameters (i.e., $\alpha \sim -\beta$) for these data. This, in turn, implies the relationship $(\mu_n + \mu_p) \sim$ const. This relationship is also suggested using the quantum-statistical-model (QSM) calculation in Ref. [15]. Inserting this relationship into Eq. (2), one can get

$$Y(A, I) \sim C A^{-\tau} \exp\left\{ \frac{F(A, I, T, \rho) + \mu_n I + cZ}{T} + N \ln(N/A) + Z \ln(Z/A) \right\}, \quad (4)$$

where $\mu_n + \mu_p = c$. The I dependence of the yield for a given isotope between different reactions 1 and 2 comes through $\Delta\mu_n = \mu_n^1 - \mu_n^2$. In the following, we take $\mu_n/T = k_1 I[(Z/A)_{\rm sys} - 0.5] + \mu_n^0/T$, in which k_1 is a parameter determined by minimizing the spread of the data for different I values. The quantity μ_n^0 is the chemical potential for symmetric $(N = Z)$ systems. By minimizing the spread in Fig. 5 and those corresponding to the other I values, $k_1 = -10.3 \pm 0.4$ is obtained. It is worth noting that the k value extracted from the experiment is consistent with the QSM-calculated slope of μ_n for different N/Z systems given in Fig. 4 of Ref. [15]. The QSM calculations also show a roughly linear dependence of μ_n or μ_p on the ratio N/Z of the system. From that figure, one can get $k_{\rm cal} = {\rm slope}/T \sim [\mu_n^1(Z/A = 0.5) - \mu_n^2(Z/A = 0.4)]T^{-1}[(Z/A)^1 - (Z/A)^2]^{-1} \sim -10$ for $T = 5$ and $\rho = 0.3\rho_0$. (In the figure, the values are given as a function of N/Z.) The calculated slope depends slightly on the temperature and density of the emitting source; namely, at $T = 5$, $k_{\rm cal} \sim -8$ for $\rho = 0.1\rho_0$ and $k_{\rm cal} \sim -12$ for $\rho = 0.5\rho_0$.

V. DISCUSSION

The corrected isotope yields are shown in the left column of Fig. 6 for $I = -1$ to 3 from the top to the bottom, including $I = 0$. For all cases, the isotope distributions are characterized by a power law distribution, although the spread for $I = 3$ is slightly larger and the quality of the fit decreases. The extracted experimental τ values $\tau_{\rm expt}$ decrease systematically from 3.9 to 1.0 as the I value increases from -1 to 3 for the corrected isotope yields.

An almost identical power law behavior is observed for the corrected isotope-yield distributions for the different reaction systems studied here. Those distributions with $|I| = 0$ and 1 are essentially identical. The results indicate that the production mechanisms of these IMFs, selected by the detector setting at 20° and the IV source component, are very similar, as mentioned earlier. This is consistent with our previous observation of energy spectra of light charged particles, measured at 38°–52° for ^{12}C + ^{116}Sn, ^{20}Ne + Ag, ^{40}Ar + ^{100}Mo, and ^{64}Zn + ^{89}Y at 47 A MeV [28]. For different

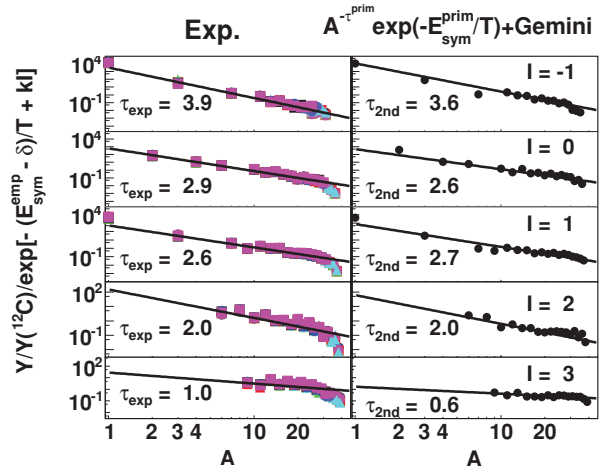

FIG. 6. (Color online) (Left) Corrected experimental isotope distributions for $I = -1$ to 3 from top to bottom for all 13 reactions. The experimental yields are corrected by $\exp[-(E_{\rm sym} - \delta)/T + kI]$, where $k = k_1[(Z/A)_{\rm sys} - 0.5]$. The pairing-term correction δ is made only for $I = 0$ and 2. Solid lines are the results by the $A^{-\tau}$ fit for $1 \leqslant A \leqslant 30$. The extracted τ values are given in each figure. (Right) Corrected calculated isotope distributions for $\tau^{\rm prim} = 2.3$. The same corrections as on the left are made. The extracted τ values are also given in each figure.

reaction systems studied at the same incident energy per nucleon, individual light-charged-particle energy spectra show almost identical shapes (Fig. 6 of Ref. [28]). In the observed angles, the intermediate-velocity source component dominates. The present results suggest that, for semiviolent collisions, the observed heavier IMF ejectiles are also produced in the participant-matter region.

In order to elucidate the observation of systematic change in the extracted τ values, a simple deexcitation model simulation was made. The simulation is based on the observation of the power law distribution for $I = 0$ isotopes in Fig. 4. This suggests that the distribution is dominated by the $A^{-\tau}$ term and the A dependence of $F(A, I = 0, T, \rho) + \mu_n N + \mu_p Z$ term is small in Eq. (2). We extend this assumption to $I \neq 0$ isotopes; that is, the primary isotope yields are generated by

$$Y(A, I) \sim A^{-\tau} \exp\left(-a_{\rm sym}^{\rm prim} I^2 A^{-1} T^{-1}\right), \quad (5)$$

where $a_{\rm sym}^{\rm prim}$ is the symmetry energy coefficient of the primary fragments. In the equation, the symmetry-energy-term dependence is kept, although in Fig. 6 the symmetry energy term has been corrected using Eq. (1). This is because the value of I is not conserved during the deexcitation process and, therefore, the symmetry-energy-term corrections, $\exp(-E_{\rm sym}^{\rm emp}/T)$ and $\exp(-E_{\rm sym}^{\rm prim}/T)$, are made independently. For comparison to these results, we have carried out a simple model simulation. In the simulation, we assigned $a_{\rm sym}^{\rm prim}/T = 5$ from Refs. [17,18] and the pairing term is neglected in the primary distribution. We then assume $\tau^{\rm prim} = 2.3$ and generate primary isotope yields for $1 \leqslant A \leqslant 50$ and $-2 \leqslant I \leqslant 5$, according to Eq. (5).

For each fragment, an excitation energy Ex of 3 A MeV is taken [11,13]. (Very similar results are obtained for $2.5 \leqslant Ex \leqslant 5.0$ A MeV. For $Ex \leqslant 2.0$ the extracted τ value starts

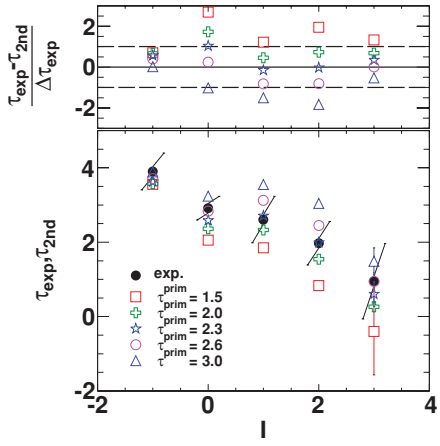

FIG. 7. (Color online) Extracted τ values from the experiment and the final products of the simulations. The experimental results are shown by dots and, for simulations, different symbols represent results from the simulations with the different τ^{prim} values, which are indicated in the figure.

to decrease notably.) The statistical deexcitation of these fragments is then followed with the GEMINI code. Here we adopted GEMINI code, since AMD + GEMINI simulations have been used in several experiments in the intermediate energy domain and reasonable agreement with many observables have been obtained [22,29–33]. The intrinsic angular momenta are set to 0 for all IMFs. The same treatment that was applied to the experimental yields has been made for the final product yields obtained with this model. The resultant distributions are plotted in the right-side column of Fig. 6. The extracted τ values $\tau_{2\text{nd}}$ are given in the figure. The experimental variation of τ values with I are well reproduced by the assumption that $\tau^{\text{prim}} = 2.3$ for the primary fragments. Different τ^{prim} values ranging from 1.5 to 3.0 for the primary isotope distribution have also been examined and the results are summarized at the bottom of Fig. 7. The spread of the experimental values represent the fact that each point for a given A consists of 13 data points. The experimental τ values are in agreement with those from the simulated events with the primary τ values in $2.0 \leqslant \tau^{\text{prim}} \leqslant 2.6$. To determine the best values, the ratio of the difference between τ_{expt} and $\tau_{2\text{nd}}$ to the experimental error is plotted at the top of the figure. From this figure, the best-fit value for the model is obtained with $\tau^{\text{prim}} = 2.4 \pm 0.2$ for the primary fragment distribution.

VI. SUMMARY

A variety of heavy ion reactions at 40 A MeV have been investigated with a focus on the power law behavior of isotope yield distributions. Violent and semiviolent collisions were selected by setting the IMF detector angle at 20°. A further isolation mechanism consisted of selecting the intermediate-velocity source component. After corrections for secondary decay effects, the yield distributions for isotopes of different $I = N - Z$ from 13 different reactions exhibit power law distributions as a function of mass number. The similarity of the distribution over different reaction systems suggests that the observed IMFs originate from a common reaction mechanism. The extracted τ values show a systematic change from 3.9 to 1.0 when the I value of the isotope changes from -1 to 3, and these values are well reproduced by a simple deexcitation model assuming that the isotopic yields of the primary distribution obey a power law dependence with a symmetry-term contribution. The experimentally extracted τ values for each I value are in good agreement with those evaluated from simulations with $\tau^{\text{prim}} \sim 2.3$, suggesting that the emitting source of the primary isotopes produced in these reactions is at, or near, the critical point.

ACKNOWLEDGMENTS

We thank the staff of the Texas A&M Cyclotron facility for their support during the experiment. We thank L. Sobotka for letting us to use their spherical scattering chamber. We also thank A. Ono and R. Charity for letting us to use their calculation codes. This work is supported by the US Department of Energy under Grant No. DE-FG03-93ER40773 and the Robert A. Welch Foundation under Grant A0330. One of us (Z. Chen) also thanks the "100 Persons Project" of the Chinese Academy of Sciences for support.

[1] J. E. Finn *et al.*, Phys. Rev. Lett. **49**, 1321 (1982).
[2] R. W. Minich *et al.*, Phys. Lett. B **118**, 458 (1982).
[3] A. S. Hirsch *et al.*, Phys. Rev. C **29**, 508 (1984).
[4] W. Trautmann, U. Milkan, U. Lynen, and J. Pochodzalla, Z. Phys. A **344**, 447 (1993).
[5] A. Bonasera *et al.*, Riv. Nuovo Cimento **23**, 1 (2000).
[6] O. Lopez *et al.*, Eur. Phys. J. A **30**, 263 (2006).
[7] M. L. Gilkes *et al.*, Phys. Rev. Lett. **73**, 1590 (1994).
[8] J. B. Elliott *et al.*, Phys. Rev. C **62**, 064603 (2000).
[9] J. B. Elliott *et al.*, Phys. Rev. Lett. **88**, 042701 (2002).
[10] J. B. Elliott *et al.*, Phys. Rev. C **67**, 024609 (2003).
[11] N. Marie *et al.*, Phys. Rev. C **58**, 256 (1998).
[12] P. Staszel *et al.*, Phys. Rev. C **63**, 064610 (2001).
[13] S. Hudan *et al.*, Phys. Rev. C **67**, 064613 (2003).
[14] M. B. Tsang *et al.*, Phys. Rev. C **64**, 054615 (2001).
[15] A. S. Botvina, O. V. Lozhkin, and W. Trautmann, Phys. Rev. C **65**, 044610 (2002).
[16] M. B. Tsang, Eur. Phys. J. A **30**, 129 (2006).
[17] M. Huang *et al.*, Phys. Rev. C **81**, 044620 (2010).
[18] Z. Chen *et al.*, Phys. Rev. C **81**, 064613 (2010).
[19] A. Ono and H. Horiuchi, Phys. Rev. C **53**, 2958 (1996).
[20] A. Ono, Phys. Rev. C **59**, 853 (1999).
[21] R. J. Charity *et al.*, Nucl. Phys. A **483**, 371 (1988).
[22] R. Wada *et al.*, Phys. Rev. C **69**, 044610 (2004).
[23] M. E. Fisher, Rep. Prog. Phys. **30**, 615 (1967).
[24] M. A. Preston, *Physics of the Nucleus* (Addison-Wesley, Reading, MA, 1962), chpt. 7.
[25] M. V. Ricciardi *et al.*, Nucl. Phys. A **733**, 299 (2004).

[26] M. V. Ricciardi *et al.*, Nucl. Phys. A **749**, 122c (2005).
[27] M. Huang *et al.*, Nucl. Phys. A **847**, 233 (2010).
[28] K. Hagel *et al.*, Phys. Rev. C **62**, 034607 (2000).
[29] R. Wada *et al.*, Phys. Lett. B **422**, 6 (1998).
[30] R. Wada *et al.*, Phys. Rev. C **62**, 034601 (2000).
[31] A. Ono, S. Hudan, A. Chbihi, and J. D. Frankland, Phys. Rev. C **66**, 014603 (2002).
[32] A. Ono and H. Horiuchi, Prog. Part. Nucl. Phys. **53**, 501 (2004).
[33] S. Hudan, R. T. de Souza, and A. Ono, Phys. Rev. C **73**, 054602 (2006).